Mathematical modelization of fixed-bed corn drying and experimental validation

Sébastien Janas [a] Phidias Dzaomuho [b] Emeline Verdin [c]
Nicolas Jacquet [e] Paul Malumba [d] Michel Crine [c]
François Béra [a]

[a] *University of Liege, Gembloux Agro-Bio Tech, Food Process Engineering Laboratory, Belgium*

[b] *University of Liege, Gembloux Agro-Bio Tech, Quality and Products Safety Laboratory, Belgium*

[c] *University of Liege, Laboratory of Chemical Engineering, Belgium*

[d] *Kinshasa University, Faculty of Agricultural Sciences, Congo*

[e] *University of Liege, Gembloux Agro-Bio Tech, Department of Industrial Biological Chemistry, Belgium*

Abstract

This work presents a new model of heat and mass transfers during fixed-bed corn drying. The fixed-bed is divided into a number of perfectly mixed stages. The temperature and moisture content of the drying air and the temperature of the grains are described by 3 ordinary differential equations (ODEs) and solved by a third-order implicit method. The evolution of the grain moisture content is obtained by solving the Fick equation in 3D on a real grain geometry by the finite element method. The model correctly describes the evolution of corn moisture content during fixed-bed drying with constant drying air temperatures of $50°C$, $75°C$, and $90°C$ and with air velocities of 0.5 $m\ s^{-1}$, 0.9 $m\ s^{-1}$, and 1.15 $m\ s^{-1}$.

Key words: Corn, Finite element method, Fixed-bed drying, Heat and mass transfer, Modelization

a	Specific surface area ($m^2\ m^{-3}$)
a_w	Water activity (-)
C_{GAB}	Parameter of the GAB model (-)

Email address: janas.sebastien@gmail.com (Sébastien Janas).

Cp	Specific heat ($J\ kg^{-1}\ ^{\circ}C^{-1}$)
D_{eff}	Water effective diffusivity ($m\ s^{-2}$)
dx	Height of a bed layer (m)
h	Mass transfer coefficient ($m\ s^{-1}$)
Hw	Latent heat of water evaporation ($J\ kg^{-1}$)
K	Parameter of the GAB model (-)
k	Heat transfer coefficient ($J\ m^{-2}\ ^{\circ}C^{-1}\ s^{-1}$)
S	Surface of a bed layer (m^2)
T	Grain Temperature ($^{\circ}C$)
U	Air Temperature ($^{\circ}C$)
U_h	Discretized solution of the PDE (-)
V	Air velocity ($m\ s^{-1}$)
W	Weight (kg)
X	Grain Moisture content (d.b.)
X_{mg}	Parameter of the GAB model (-)
Y	Air moisture content (kg water kg^{-1} dry air)

Greek symbols

ρ	Density (kg m^{-3})
ϵ	Porosity (-)
τ	Shape function (-)
Ω	Entire domain of the FEM model (-)
Γ	Boundary of the FEM model (-)

Subscripts

$_v$	Relative to the vapor water
$_w$	Relative to the liquid water
$_{eq}$	In equilibrium
$_a$	Relative to the air

$_s$ Relative to the solid part of the bed

1 Introduction

Since 2001, corn (Zea mays L.) is reported on the FAOSTAT website as the first crop in the world, before rice and wheat. At the time of harvest, corn has a moisture content too high for storage (between 30% and 40% w.b.), and has to be dried.

During drying, the corn kernel undergoes cracking [1–3], protein denaturation [4,5], changes in functional properties of wet-milled starch granules [6], and loss of wet-milling properties [7]. To control the impact of drying on food characteristics, it is necessary to monitor accurately the spatial distribution of temperature and moisture content, and quality losses in relation to these two factors.

Corn drying is often done in fixed-beds because of their simplicity. Unfortunately, the heterogeneity of the air and grain temperature and moisture content during the process makes it hard to optimize the process. Modelization of heat and mass transfers during fixed-bed drying of corn is certainly of great help in this context. Several models of fixed-bed corn drying are described in the literature [8–11]. In most of them, the temperature and moisture content for each grain are assumed to be homogeneous. This approach is insufficient when the goal is to accurately monitor quality properties of the grains (e.g. protein denaturation) located in specific parts of the kernel (germ or endosperm). The most advanced models available in the literature describe the grains as perfect spheres, making it possible to solve the Fick equation at each point in the bed [10,11]. The drawback of this approach is that grain kernels are not perfect spheres, and that this kind of approximation cannot help to monitor the moisture content in specific parts of the kernel.

In this work, the bed is divided into several ideally mixed stages where air and grain properties are assumed to be homogeneous. The assumption of perfectly mixed stages is supported by the relatively high Reynolds numbers in fixed-beds, leading to turbulent regimes accompanied by some mixing of the air around the product [12]. For each stage, the air temperature, air moisture content, and grain temperature are described by simple balances across the stage, leading to a system of ordinary differential equations (ODEs) which can be solved by an implicit method. The evolution of the grain moisture content

is obtained by solving the Fick equation in 3D on real grain geometry by the finite element method.

2 Materials and methods

2.1 Fixed-bed drying of corn

The corn kernel used was a flint corn, of the Baltimore variety. The moisture content at harvest was about 40% w.b. Directly after harvesting the corn was stored at -20°C in plastic bags until drying. Drying curves did not show any change from the day of harvest to the end of the trials. Before each drying, the required quantity of corn was equilibrated at laboratory temperature for one night.
A schematic view of the laboratory fixed-bed dryer used for the experiments is presented in Figure 1. This dryer is composed of a polycarbonate tube from VINK (Belgium) (height = 0.6 m and diameter = 0.12 m), into which air was introduced from the bottom at fixed temperature and superficial velocity. During this process, the air temperature, relative humidity, and velocity were measured downstream of the drying chamber, and air temperature and relative humidity were measured upstream. The temperature was also measured along the central axis of the bed every 5 cm from the bottom to the top of the bed. Temperatures were measured with type T TT-T-30-SLE thermocouples from OMEGA (England), air relative humidity with TR200 probes from NOVASINA (Switzerland), and air velocity with a TEST0 445 anemometer (Germany). Thermocouple and air humidity probe signals were measured with a 3595551H UNIVERSAL IMP from SOLARTRON (England), and recorded with a program written in LABVIEW 5.1. Air velocity data were recorded with the TESTO LOGICIEL-COMFORT "Light" interface.

The moisture content was measured at the beginning and end of the process on ± 5g of grains by differential weighing after 48 h at 105°C. During these trials, the tube was regularly weighed to get the mean bed moisture content, and the height of the bed was measured to get a relationship between the shrinkage of the bed and its moisture content. All trials were done in triplicate.

The trials were performed with air temperature in the range 50°C - 90°C and air velocity in the range 0.5 $m\ s^{-1}$ - 1.15 $m\ s^{-1}$. To check that these air velocities correspond to fixed-bed drying, the evolution of the pressure drop through the bed was measured under these conditions.

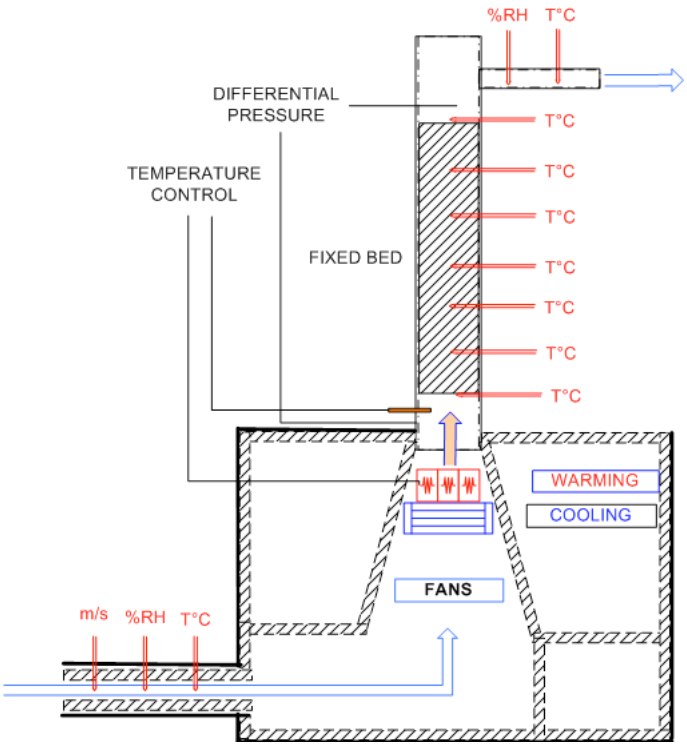

Fig. 1. Schematic view of the dryer used for the trials.

2.2 Determination of the pressure drop through the bed

A corn sample was put in the drying chamber to get a bed height of 0.4 m, representing about 3.0 kg of grains. Air at $30°C$ was introduced from the bottom of the dryer at a velocity of 0.5 $m\ s^{-1}$. The pressure drop through the bed was measured with a CAT NO 2030 differential manometer from Magnehelic (U.S.A). The air velocity was increased by 0.1 $m\ s^{-1}$ steps to 1.15 $m\ s^{-1}$ and the pressure drop was measured teach step.

2.3 Mathematical modeling of fixed-bed drying

The hypotheses of the model are :

- The bed is divided into several ideally mixed stages, called *layers*, in which air and grain properties are assumed to be homogeneous. The assumption of perfectly mixed stages is supported by the relatively high Reynolds numbers in fixed-beds, leading to turbulent regimes accompanied by mixing of the air around the product [12];
- The air temperature, air moisture content, grain temperature, and mean grain moisture content are homogeneous in each layer;
- For each layer, the air temperature, air moisture content, and grain temper-

ature are described by simple balances across the layer, leading to a system of ODEs which can be solved by an implicit method;
- The Fick equation is used in each layer to describe the evolution of the grain moisture content;
- The walls of the bed are isolated;
- There is no heat or mass transfer between grains;
- The air velocity is constant.

2.3.1 Air temperature

The total power entering the i-th layer with the drying air is equal to

$$\epsilon \rho_a V S \left[(Cp_a + Cp_v Y_{i-1}) U_{i-1} \right] \tag{1}$$

and the total power leaving the i-th layer with the drying air is

$$-\epsilon \rho_a V S \left[(Cp_a + Cp_v Y_i) U_i \right] \tag{2}$$

The power transferred from the air to the grains can be modeled as

$$-kaSdx \left(U_i - T_i \right) \tag{3}$$

The rate of variation of energy in the air contained in the i-th layer is equal to

$$\rho_a \epsilon \left(Cp_a + Cp_v Y_i \right) \frac{\delta U_i}{\delta t} Sdx \tag{4}$$

These terms give the final expression of the energy balance for the i-th layer

$$\begin{aligned} \rho_a \epsilon \left(Cp_a + Cp_v Y_i \right) \frac{\delta U_i}{\delta t} = & \quad -ka \left(U_i - T_i \right) && (5) \\ & + \frac{\epsilon \rho_a V}{dx} \left[(Cp_a + Cp_v Y_{i-1}) U_{i-1} \right] && (6) \\ & - \quad \frac{\epsilon \rho_a V}{dx} \left[(Cp_a + Cp_v Y_i) U_i \right] && (7) \end{aligned}$$

2.3.2 Air moisture content

The moisture entering the i-th layer with the drying air is equal to

$$\epsilon \rho_a V S Y_{i-1} \tag{8}$$

and the moisture leaving it is

$$-\epsilon \rho_a V S Y_i \tag{9}$$

The moisture entering the air of the i-th layer by dehydration of the grains can be modeled as

$$-\frac{\delta X_i}{\delta t} \rho_{db} S dx (1 - \epsilon) \tag{10}$$

The total variation of air moisture content in the air of the i-th layer is given by

$$\epsilon \rho_a S dx \frac{\delta Y_i}{\delta t} \tag{11}$$

These terms give the final expression of the air moisture balance for the i-th layer

$$\begin{aligned} \epsilon \rho_a \frac{\delta Y_i}{\delta t} = & -\frac{\delta X_i}{\delta t} \rho_{db} (1 - \epsilon) && (12) \\ & + \epsilon \rho_a V S Y_{i-1} && (13) \\ & - \epsilon \rho_a V S Y_i && (14) \end{aligned}$$

2.3.3 Grain temperature

The energy transferred to the grains in the i-th layer from the air is equal to

$$ka \left(U_i - T_i \right) S dx \tag{15}$$

The energy leaving the grains in the i-th layer through vaporization of water is equal to

$$\frac{\delta X_i}{\delta t} \rho_{db} S dx (1 - \epsilon) H w \tag{16}$$

The total energy variation in the grains contained in the i-th layer is

$$(1-\epsilon)\rho_s Cp_s S dx \frac{\delta T_i}{\delta t} \tag{17}$$

These terms give the final expression of the energy balance for the grains in the i-th layer

$$(1-\epsilon)\rho_s Cp_s \frac{\delta T_i}{\delta t} = \quad ka\,(U_i - T_i) \tag{18}$$

$$+ \frac{\delta X_i}{\delta t}\rho_{db}(1-\epsilon)Hw \tag{19}$$

2.3.4 Grain moisture content

Water diffusion in a grain can be described by Fick's second law [13]

$$\frac{\delta X}{\delta t} = \overrightarrow{\nabla} \cdot (D_{eff}\overrightarrow{\nabla} X) \tag{20}$$

The balance between the water flux from the product core to its surface and the vapor removed by air can be written as

$$-\vec{n}\rho_{db} \cdot (D_{eff}\overrightarrow{\nabla} X) = h\rho_a(X_{eq} - X) \tag{21}$$

where X_{eq} is the equilibrium grain moisture content given by its sorption/desorption isotherm.

2.4 Numerical methods

2.4.1 The system of ODEs

The equations describing the air temperature, air moisture content, and grain temperature are a system of ordinary differential equations of the form

$$\frac{\delta Z}{\delta t} = F(Z,t) \tag{22}$$

This kind of equation can be solved by explicit or implicit methods. In this work, an implicit third-order backward differentiation method is used [14].

$$\frac{Z^{n+1} - \frac{1}{11}(18Z^n - 9Z^{n-1} + 2Z^{n-2})}{\Delta t} = \frac{6}{11}F^{n+1} \tag{23}$$

This method requires more memory for the resolution of the system because the solutions have to be stored for 3 time steps.

For air temperature, the discretized equation becomes

$$U_i^{n+1} - \frac{6}{11}\Delta t \left[\frac{-ka(U_i^{n+1} - T_i^{n+1})}{\rho_a \epsilon (Cp_a + Cp_v Y_i^{n+1})} + \frac{V(Cp_a + Cp_v Y_{i-1}^{n+1})U_{i-1}^{n+1}}{(Cp_a + Cp_v Y_i^{n+1})dx} - \frac{VU_i^{n+1}}{dx}\right] = \frac{1}{11}\left(18U_i^n - 9U_i^{n-1} + 2U_i^{n-2}\right) \tag{24}$$

For air moisture content

$$Y_i^{n+1} - \frac{6}{11}\Delta t \left[\frac{-(1-\epsilon)\rho_{db}\frac{\delta X_i}{\delta t}}{\epsilon \rho_a} + \frac{V(Y_{i-1}^{n+1} - Y_i^{n+1})}{dx}\right] = \frac{1}{11}\left(18Y_i^n - 9Y_i^{n-1} + 2Y_i^{n-2}\right] \tag{25}$$

And for grain temperature

$$T_i^{n+1} - \frac{6}{11}\Delta t \left[\frac{ka(U_i^{n+1} - T_i^{n+1})}{(1-\epsilon)\rho_s Cp_s} + \frac{\rho_{db} H w \frac{\delta X_i}{\delta t}}{\rho_s Cp_s}\right] = \frac{1}{11}\left(18T_i^n - 9T_i^{n-1} + 2T_i^{n-2}\right) \tag{26}$$

For the first layer, the U_{i-1} and Y_{i-1} values are respectively the air temperature and moisture content at the inlet of the dryer.

The discretization leads to a linear system of $3n$ equations, where n is the number of layers in the bed. This system must be built and solved for each time step.

2.4.2 The grain moisture PDE

The grain moisture equation is a partial differential equation which is solved by the finite element method.

In the finite element method, the approximated form U_h of the solution U of a PDE is written as a polynomial approximation

$$U_h = \sum_{i=1}^{n} \tau_i U_i \tag{27}$$

where n is the number of nodes in the domain and τ_i are the shape functions.

By replacing the solution U of the PDE by its approximate form U_h, a residual can be defined

$$R = E(U_h) \tag{28}$$

where E is the equation considered.

The goal of the finite element method is to find the values of U_h which minimize the residual. In particular, the Galerkin method consists in finding the value of U_h minimizing the product of the residual by the shape functions τ_i over the entire domain.

$$\forall i = 1...n \int_{\Omega} \tau_i \; R \; d\Omega = 0 \tag{29}$$

For the Fick equation, the residual can be written as

$$R = \frac{\delta X_h}{\delta t} - \overrightarrow{\nabla} \cdot \left(D_{eff} \overrightarrow{\nabla} X_h \right) \tag{30}$$

And the Galerkin formulation as

$$\forall i = 1...n \int_{\Omega} \tau_i \left[\frac{\delta X_h}{\delta t} - \overrightarrow{\nabla} \cdot \left(D_{eff} \overrightarrow{\nabla} X_h \right) \right] d\Omega = 0 \tag{31}$$

Which gives

$$\forall i = 1...n \ \int_\Omega \tau_i \frac{\delta X_h}{\delta t} d\Omega - \int_\Omega \tau_i \overrightarrow{\nabla} \cdot \left(D_{eff} \overrightarrow{\nabla} X_h \right) d\Omega = 0 \tag{32}$$

The second term can be transformed using integration by parts [1].

$$\forall i = 1...n \ \int_\Omega \tau_i \frac{\delta X_h}{\delta t} d\Omega + \int_\Omega (\overrightarrow{\nabla} \tau_i) D_{eff} (\overrightarrow{\nabla} X_h) d\Omega - \int_\Omega \overrightarrow{\nabla} \cdot (\tau_i D_{eff} \overrightarrow{\nabla} X_h) d\Omega = 0 \tag{33}$$

The divergence theorem [2] is then used on the last term.

$$\forall i = 1...n \ \int_\Omega \tau_i \frac{\delta X_h}{\delta t} d\Omega + \int_\Omega (\overrightarrow{\nabla} \tau_i) D_{eff} (\overrightarrow{\nabla} X_h) d\Omega - \int_\Gamma \vec{n} \cdot (\tau_i D_{eff} \overrightarrow{\nabla} X_h) d\Gamma = 0 \tag{34}$$

Equation 21 is used to replace the last term

$$\forall i = 1...n \ \int_\Omega \tau_i \frac{\delta X_h}{\delta t} d\Omega + \int_\Omega (\overrightarrow{\nabla} \tau_i) D_{eff} (\overrightarrow{\nabla} X_h) d\Omega + \int_\Gamma \tau_i h (X - X_{eq}) d\Gamma = 0 \tag{35}$$

X_h is replaced with its definition.

$$\forall i = 1...n \ \sum_{j=1}^{n} \int_\Omega \tau_i \tau_j d\Omega \ \frac{\delta X_j}{\delta t} + \sum_{j=1}^{n} \int_\Omega (\overrightarrow{\nabla} \tau_i) D_{eff} (\overrightarrow{\nabla} \tau_j) d\Omega \ X_j + \sum_{j=1}^{n} \int_\Gamma \tau_i h \tau_j d\Gamma = \int_\Gamma \tau_i h X_{eq} d\Gamma \tag{36}$$

Defining K_{ij}, M_{ij}, S_{ij} and F_i as

$$K_{(i,j)} = \int_\Omega \tau_i a \tau_j d\Omega$$
$$M_{(i,j)} = \int_\Omega (\overrightarrow{\nabla} \tau_i) D_{eff} (\overrightarrow{\nabla} \tau_j) d\Omega$$
$$S_{(i,j)} = \int_\Gamma \tau_i h \tau_j d\Gamma$$
$$F_{(i)} = \int_\Gamma \tau_i h X_{eq} d\Gamma$$

[1] (fg)'=f'g+fg' and so f'g=(fg)'-f'g

[2] $\int_\Omega \overrightarrow{\nabla} \cdot f \ d\Omega = \int_\Gamma \vec{n} \cdot f \ d\Gamma$

The linear system can be written as

$$\forall i = 1...n \sum_{j=1}^{n} K_{(i,j)} \frac{\delta X_j}{\delta t} + \sum_{j=1}^{n} M_{(i,j)} X_j + \sum_{j=1}^{n} S_{(i,j)} X_j = F_{(i)} \tag{37}$$

The temporal derivative of the moisture content is discretized by a backward Euler method

$$\frac{\delta X_j}{\delta t} = \frac{X_j^t - X_j^{t-1}}{\Delta t} \tag{38}$$

which gives for the linear system

$$\forall i = 1...n \sum_{j=1}^{n} K_{(i,j)} X_j^t = \sum_{j=1}^{n} (K_{(i,j)} - \Delta t M_{(i,j)} - \Delta t S_{(i,j)}) X_j^{t-1} + \Delta t F_{(i)} \tag{39}$$

2.4.3 Shrinkage phenomena

To take shrinkage phenomena into account, the size of each layer was adjusted at each time step, according to the local moisture content.

2.4.4 Condensation phenomena

When the air moisture content is higher than its saturation moisture content, it is assumed in this model that the excess of water condense directly on the grains, resulting in a proportional increase in grains moisture content.

2.4.5 Implementation of the method

The model was written in C++. The linear system obtained by resolving the ODEs at each time step was solved with the GMRES solver interface of the GMM++ library. The finite element model was written with the help of the Getfem++ library.

2.5 Determination of the physical parameters required by the model

2.5.1 Sorption isotherm

The samples were equilibrated at different a_w values. To this end, 5 saturated salt solutions were selected: $MgCl_2$, K_2C0_3, $NaBr$, $NaCl$, and KCl. The analyses were also conducted on fresh and lyophilized corn. When the samples were in equilibrium, their moisture contents were determined by measuring the weight lost through oven drying at $105°C$ for 48h. The a_w was measured at $20°C$ with an Aqualab hygrometer. Samples were analyzed at least in triplicate.
To model the experimental data, the Guggenheim, Anderson and de Boer (GAB) model was used.

$$X = \frac{X_{mg}\ K\ C_{GAB}\ a_w}{(1 - K\ a_w)(1 - K\ a_w + C_{GAB}\ K\ a_w)} \tag{40}$$

Parameter values were determined by nonlinear regression on the experimental values with the help of the statistical R software [15].

2.5.2 Determination of the effective diffusivity of water

To get the effective diffusivity of water, the drying procedure was monitored on about 400 g of corn, corresponding to a bed height of 5 cm. Air temperatures of $50°C$, $75°C$, and $90°C$, and air velocities of 0.5 $m\ s^{-1}$, 0.9 $m\ s^{-1}$, and 1.15 $m\ s^{-1}$ were used. All trials were done in duplicate.
The evolutions of the moisture content observed during the thin-layer trials were used to compute the effective water diffusivity in the grains. A 3D diffusive model based on the real geometry of the flint corn used in this study was used to compute the evolution of moisture content in the grains [16], and a nonlinear regression procedure was used to estimate the effective water diffusivity minimizing the residual sum of squares between the experimental values of water content and the values predicted by the model.

2.5.3 Determination of fixed bed porosity

To measure the fixed bed porosity, the exact volume of a container 9.5 cm in diameter and 12 cm high was measured by differential weighing of distilled water. The contained was filled with each corn sample and weighed. Distilled water was added until the surface was reached before weighing a second time. The porosity of the corn bed was computed as :

$$\epsilon = \frac{W_2 - W_1}{W_w} \tag{41}$$

where W_1 and W_2 are the values of the first and second weighings, respectively, and W_w is the weight of the water filling the container entirely.
The porosities of beds of fresh corn and of dried corn were determined at different moisture contents.

2.5.4 Measurment of the bed specific surface area

The bed specific surface area was measured by X-ray microtomography. This non-invasive technique allows visualizing the internal texture of a sample on the basis of local variations of the x-ray attenuation coefficient. It was used to obtain 2-dimensional cross-section images of fixed-bed samples.

The x-ray tomographic device used in this study was a "SkyScan 1172" (SkyScan, Belgium). The cone beam source operated at 100 kV and 100 μA. The detector was a 2D, 3336 pixel x 3336 pixel, 16 bit X-ray camera with a spatial resolution of 11.8 μm. The rotation step was set at 0.2° in order to improve image quality, giving total acquisition times close to 30 minutes. For each angular position a radiograph of the whole bed, instead of a 1D projection of a cross section, was recorded by the 2D camera. Once the sample was placed in the microtomograph, scanning was performed on a height of 25 mm. Cross sections separated by 10.02 μm were reconstructed along the fixed-bed of corn with a cone beam reconstruction software. The bed sample was a plastic container (diameter = 5.5 cm, height = 5.5 cm) filled with corn grains. Tomographic measurements were performed on 4 samples, differing in moisture content.

The 2D images obtained were analyzed with the MATLAB R2008 Image Processing Toolbox. Analysis of each of the 96 pictures consisted in defining the region of interest, segregating the grains from the air, computing the total perimeter of the grains and computing the specific surface area as the ratio between the total perimeter of the grains and the total area of each picture. The specific surface area was the average of the 96 values thus calculated.

2.6 Validation of the model

The physical properties of air and corn which were not experimentally determined were found in the literature and are summarized in Table 1. For the computations, the bed was divided into 8 layers, and the time step used was

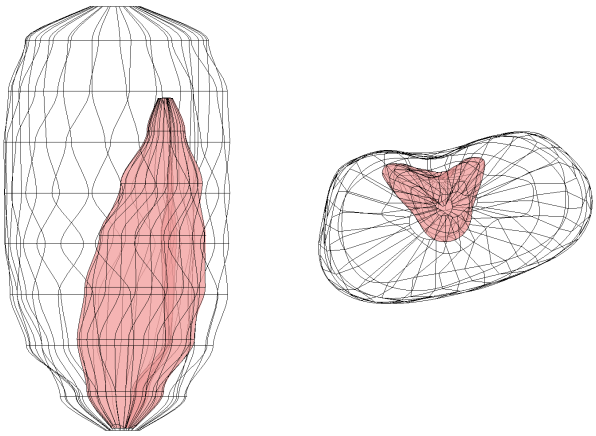

(a) View of the side (b) View of the upside

Fig. 2. 3D geometry of a maize grain. The germ is shown in red and the endosperm in white.

of 120 s. Higher accuracy in the time and space discretization did not lead to better accuracy of the solution of the model.

The corn geometry (Figure 2) was obtained by NMR imagery in a previous work [16], exported in STL format and meshed with the GMSH software.

The C++ code was compiled with GCC 4.0.1 and the computation took about 30 minutes on a MacBook Pro dualcore 2.93 Ghz.

The air temperature, moisture content, and velocity measured during experimental dryings were used to estimate the accuracy with which the model can predict the evolution of corn moisture content. For each test, the model performance was determined by it's mean error of prediction, estimated as :

$$E = \frac{1}{n} \sum_{i=1}^{n} \frac{|MOD_i - EXP_i|}{EXP_i} * 100 \tag{42}$$

where n is the number of experimental values, MOD_i and EXP_i are respectively the value given by the model and the values measured experimentally at the i-th experimental point.

Table 1. Air and corn physical properties used in the model

Property	Equation	Reference
Air density	$\rho_{air} = \frac{341.25}{(T+273)}$	[19]
Air viscosity	$\mu_{air} = 1.66 * 10^{-5} \left(\frac{T+273}{273}\right)^{0.756}$	[19]
Air specific heat	$Cp_{air} = 0.9774 + 0.1124 * 10^{-3}(T_a + 273) + 1.19035 * 10^{-7}(T_a + 273)^2$	[19]
Moisture diffusivity in the air	$D_w = \left(\frac{T}{273}\right)^{1.81}$	[19]
Corn density	1350	[11]
Corn specific heat	$Cp = 4190 \ \frac{X}{(1+X)} + 840 \ \left(1 - \frac{X}{(1+X)}\right)$	[20]
Mass transfer coefficient	$Sh = \frac{h d_g}{D_w} = 2 + 1.8 Re^{\frac{1}{2}} Sc^{\frac{1}{3}}$	[21]
Heat Transfer coefficient	$Nu = \frac{k \, d_g}{\lambda_a} = 2 + 1.8 \, Re^{\frac{1}{2}} \, Pr^{\frac{1}{3}}$	[21]

3 Results and discussion

3.1 Determination of the pressure gradient through the bed

Figure 3 presents the experimental value of the pressure gradient as a function of the air velocity. The pressure gradient increases constantly over the air velocity range tested, indicating that the fluidization regime is not reached.

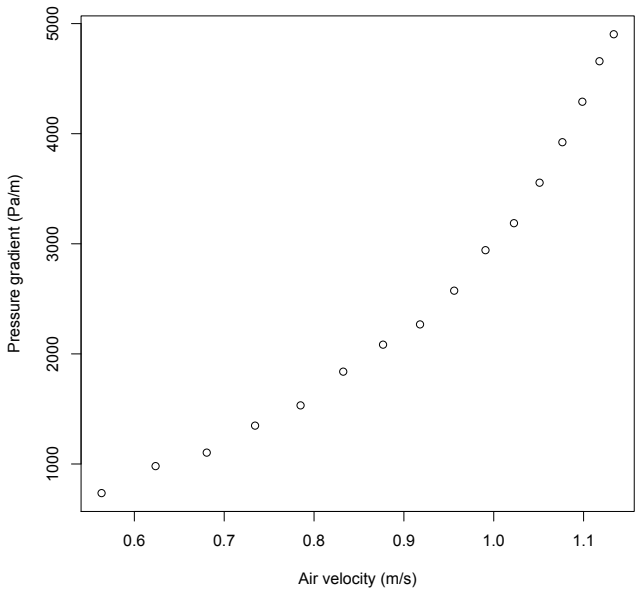

Fig. 3. Pressure gradient through the bed in function of the air velocity.

3.2 Sorption Isotherm

The experimental points and the GAB curve are presented in Figure 4. The parameters of the GAB model are reported in Table 2. The residual sum of squares between the experimental data and the values given by the GAB model is 0.0016. According to this value, the GAB model suited to fit experimental points for a flint corn isotherm.

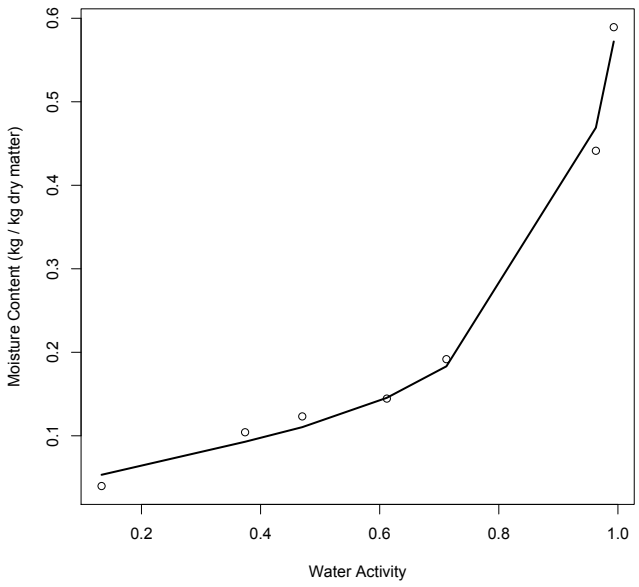

Fig. 4. Desorption isotherm of a flint corn - Experimental points and GAB model

Table 2
Parameters of the GAB model obtained by nonlinear regression on the experimental data's

Property	Value
X_{mg}	0.07055094
C_{GAB}	15.015108
k	0.884020

3.3 Determination of bed shrinkage

For the determination of bed shrinkage, 322 coupled values of heights and moisture contents of the bed were obtained (Figure 5). An adimensional relationship between the height of the bed and its moisture content was obtained by modifying the data for each time step (the height and the moisture content of the bed were divided by their respective initial values for each trial).

A linear regression gives the equation

$$H = 0.273859X + 0.728978 \tag{43}$$

with an R^2 coefficient of 0.9492.

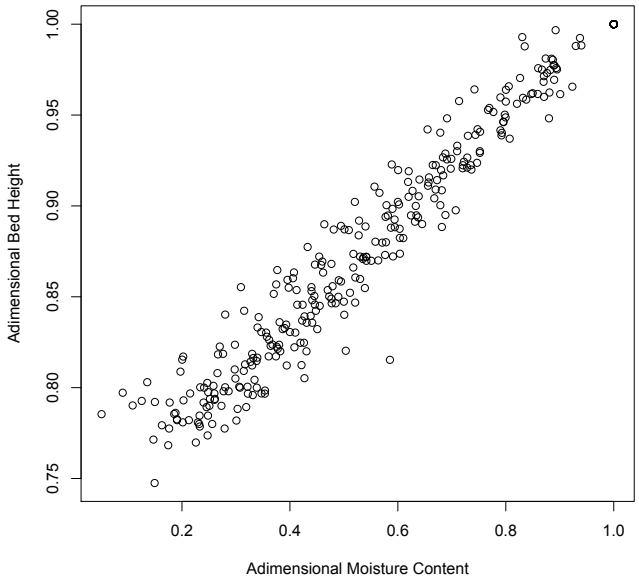

Fig. 5. Adimensional bed height in function of its adimensional moisture content, 322 experimental values

3.4 Determination of the effective diffusivity of water

Table 3 presents the value of the effective diffusivity for each temperature and velocity. The effects of the air velocity and air temperature on the effective diffusivity are not of the same order of magnitude. The greatest effect of the air velocity is a 1.24-fold effect (between the diffusivities stair velocity 0.5 $m\ s^{-1}$ and 1.15 $m\ s^{-1}$, at 90°C), whereas the greatest effect of the temperature is a 13.2-fold effect (between the diffusivities at 30°C and 90°C, at air velocity 1.15 $m\ s^{-1}$). By fitting an exponential law to the experimental data, the following equation is obtained for the effective diffusivity of flint corn during thin layer drying (the residual standard error is $9.232 * 10^{-12}$).

$$D_{eff} = 4.128 * 10^{-12} exp(0.04046T) \tag{44}$$

Table 3
Effective diffusivities computed by nonlinear regression of a 3D diffusive model on the thin layer dryings data

Temperature ($^{\circ}C$)	Air velocity (m s^{-1})	Effective diffusivity ($m^2 s^{-1}$)	Residual Error (d.b.)
30	0.5	$1.2169 * 10^{-11}$	0.0076
30	0.9	$1.2712 * 10^{-11}$	0.0049
30	1.15	$1.3580 * 10^{-11}$	0.0115
60	0.5	$5.3154 * 10^{-11}$	0.0075
60	0.9	$5.3878 * 10^{-11}$	0.0033
60	1.15	$5.4247 * 10^{-11}$	0.0107
90	0.5	$1.7647 * 10^{-10}$	0.0089
90	0.9	$1.9851 * 10^{-10}$	0.0103
90	1.15	$2.1731 * 10^{-10}$	0.0113

3.5 Determination of the fixed-bed porosity

Figure 6 presents the corn bed porosity as a function of its moisture content. The bed porosity is not influenced by its moisture content. It varies from 36.5 to 41 in the moisture range 0.05-0.55 (d.b.) and there is no clear relation between these two parameters. The best solution for modeling purposes is to use the mean value, which is 0.38 with a standard deviation of 0.011.

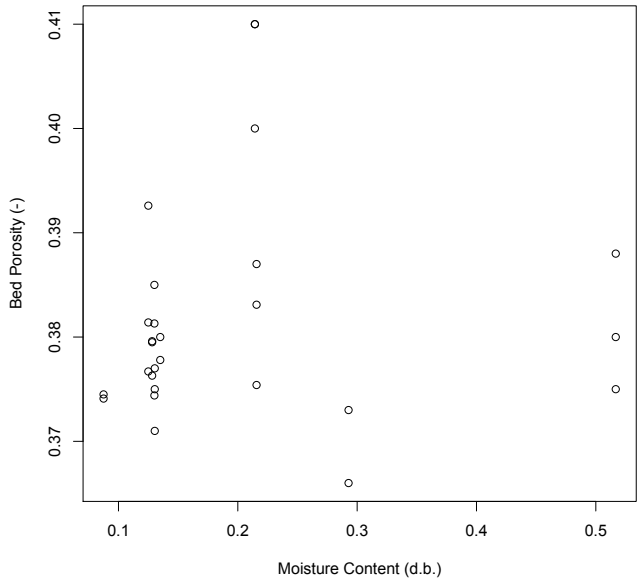

Fig. 6. Porosity of the bed in function of its moisture content, 27 experimental values.

3.6 Measurement of the bed specific surface area

Figure 7 shows a 2D picture obtained by X-ray tomography of a small corn bed. This picture is cut to get only the bed part. The specific surface area of the bed is equal to the total perimeter of the grains on a picture, divided by the picture's area.
These analyses were conducted on 4 corn samples with different moisture contents. For each sample, 92 pictures were obtained. Table 4 presents the values of the specific surface area corresponding to each moisture content.
The specific surface area of the bed increases when its moisture content decreases. The relationship between the specific surface area and the moisture content can be modeled by the following quadratic equation, with a R^2 of 0.9999.

$$a = 1258.649X^2 - 1768.593X + 1135.856 \tag{45}$$

Table 4
Specific surface of a corn bed in function of its moisture content, n=92 for each moisture content.

Moisture content (d.b)	Specific surface (m^2m^{-3})	Standard deviation
0.09	989.5	45.4
0.12	938.5	38.4
0.30	719.3	54.7
0.60	527.7	27.9

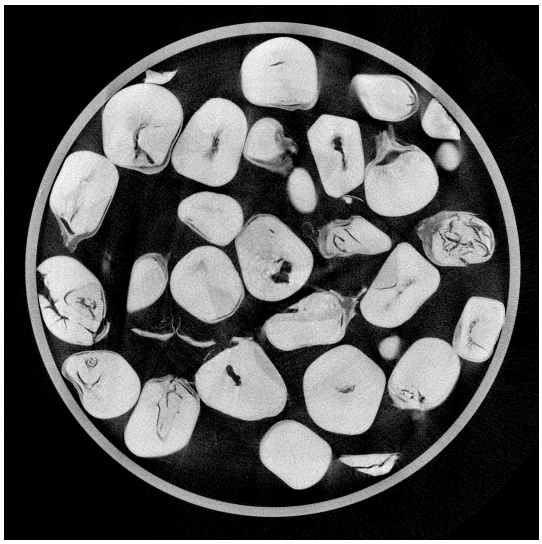

Fig. 7. 2D picture of a small corn bed obtained by X-ray tomography

3.7 Validation of the model

The mean error of prevision on all the experimental dryings is of 11%. Given the great difficulty of accurately describing the fixed-bed drying of foodstuff, an accuracy of 15% is generally considered acceptable [17].

The simulated and experimental values of the mean bed moisture content for drying trials at $75°C$ with an air velocity of 0.9 $m\ s^{-1}$ are presented in Figure 8.

The sources of error which may explain the prediction errors are :

- The use of a unique grain geometry for all layers. In practice, all grains are different. No data are available on the impact of such heterogeneity on the modelization of fixed-bed drying.
- The inaccuracy of corn physical properties.
- The inaccuracy of heat and mass transfer coefficients at the surface of grains.

These parameters are given by relations determined experimentally on other types of dryer, with other products, other air flow properties,...

- Modelization of the air flow in the bed. In this work, the air flow is assumed to be monodirectional, with perfect mixing in each layer of the bed. The high Reynolds number in fixed-beds indicates the presence of turbulences, which are generally accompanied by a non-linear shape of the flow. Modelization of such a turbulent flow in porous media is a very specialized topic [18]. No application of this theory is available yet in the field of food drying.

The advantage of the fixed-bed model presented in this paper is the possibility of tracking the moisture content inside specific parts of the grains, such as the endosperm of the germ.

Figure 9 shows the evolutions of the endosperm and germ moisture content in the first and last bed layers during drying at $75°C$ and 0.9 $m\ s^{-1}$. The dehydration rate is higher in the first layer than in the last, and the moisture content is higher in the germ than in the endosperm. Figure 10 shows the evolution of the difference bewteen the germ and endosperm moisture contents during the same drying. The difference is positive, which indicates that the moisture content is higher in the germ than in the endosperm. At the beginning of the drying, the difference increases, indicating that the rate of dehydration is higher in the endosperm. After about 1h, there is a switch in the drying rate amplitudes: the drying rate becomes higher in the germ than in the endosperm.

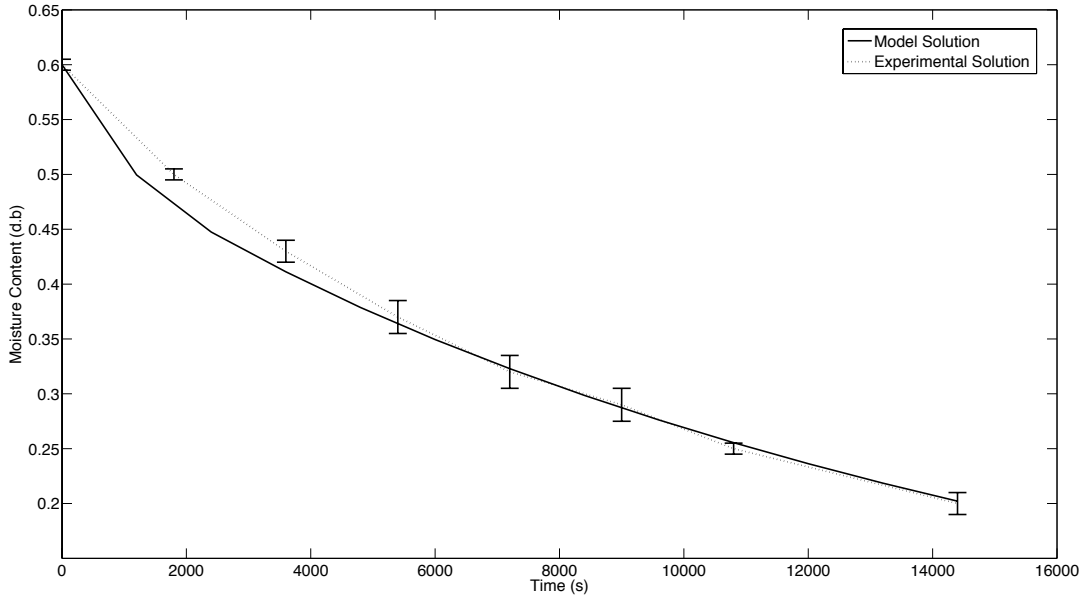

Fig. 8. Measured and calculated moisture content (d.b) for dryings at $75°C$ and 0.9 $m\ s^{-1}$.

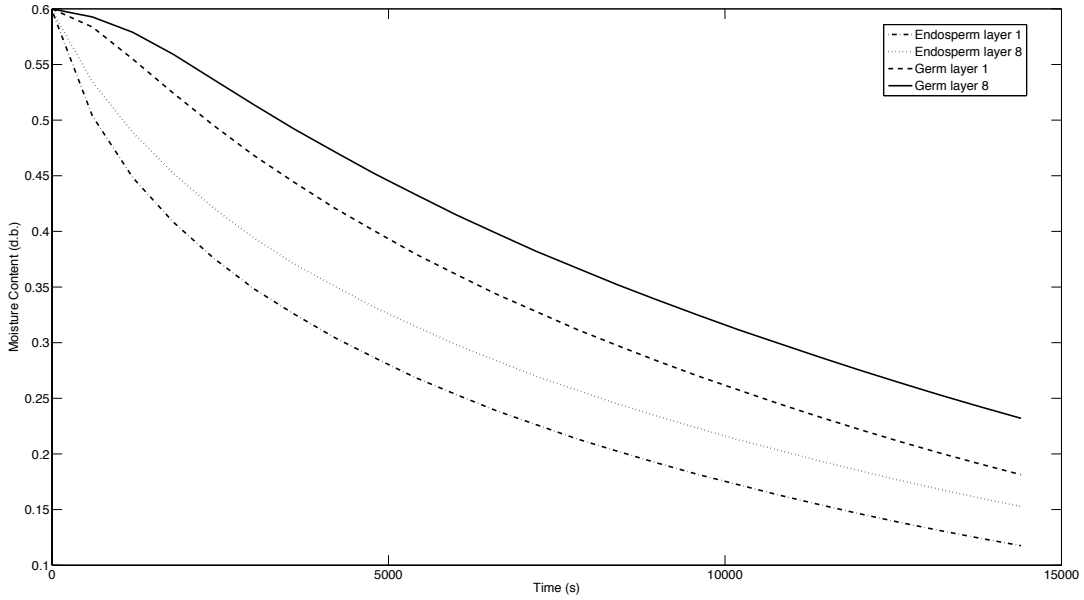

Fig. 9. Calculated moisture contents (d.b) in the germ and in the endosperm, for the first and the last bed layers, for dryings at $75°C$ and 0.9 $m\ s^{-1}$.

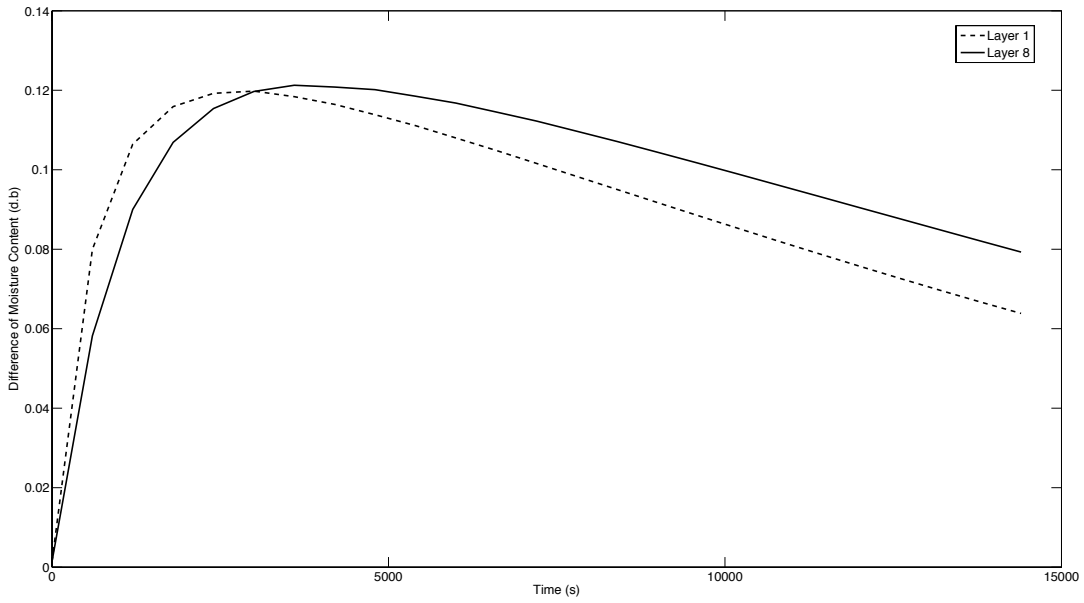

Fig. 10. Difference between the calculated moisture contents (d.b) in the germ and in the endosperm, for the first and the last bed layers, for dryings at $75°C$ and 0.9 $m\ s^{-1}$.

4 Conclusions

In this work, a new model of heat and mass transfer during fixed-bed drying of corn is presented. The temperature and moisture content of the drying air and the temperature of grains are described by 3 ODEs and solved by a third-order implicit method. The evolution of the grain moisture content is obtained

by solving the Fick equation in 3D on a real grain geometry by the finite element method. The model was applied to predicting the evolution of the corn moisture content during fixed-bed drying with three different constant drying air temperatures ($50°C$, $75°C$, and $90°C$) and three different air velocities (0.5 $m\ s^{-1}$, 0.9 $m\ s^{-1}$, and 1.15 $m\ s^{-1}$). The mean accuracy of the model is of 11%. For this type of drying, an accuracy of 15% is generally considered acceptable. The model is able to predict the evolution of moisture content in specific parts of the grains, such as the germ or the endosperm. This is certainly of interest in studying the impact of drying on grain quality characteristics specifically located in one of these parts.

Acknowledgments

S. Janas acknowledges financial support from the Fonds pour la Recherche dans l'Industrie et l'Agriculture, Belgium. He also thanks Florence Lefebvre and Guy Delimme for their help in the laboratory.

References

[1] R. J. Gustafson, D. R. Thompson, S. Sokhansanj, Temperature and stress analysis of corn kernel-finite element analysis, Transactions of the ASAE 22 (4) (1979) 955–960.

[2] V. Davidson, S. Noble, R. Brown, Effects of drying air temperature and humidity on stress cracks and breakage of maize kernels, J Agr Eng Res 77 (3) (2000) 303–308.

[3] S. Prachayawarakorn, S. Soponronnarit, S. Wetchacama, K. Chinnabun, Methodology for enhancing drying rate and improving maize quality in a fluidised-bed dryer, J Stored Prod Res 40 (4) (2004) 379–393.

[4] C. Lupano, M. Anon, Denaturation of wheat endosperm proteins during drying, Cereal Chemistry 64 (6) (1987) 437–442.

[5] P. Malumba, C. Vanderghem, C. Deroanne, F. Béra, Influence of drying temperature on the solubility, the purity of isolates and the electrophoretic patterns of corn proteins, Food Chemistry 111 (3) (2008) 564–572.

[6] P. Malumba, C. Massaux, C. Deroanne, T. Masimango, F. Béra, Influence of drying temperature on functional properties of wet-milled starch granules, Carbohydrate Polymers 75 (2) (2009) 299 – 306. doi:DOI: 10.1016/j.carbpol.2008.07.027.

[7] J. Lasseran, Incidence of drying and storing conditions of corn (maize) on its quality for starch industry, Starch 28 (8) (1973) 257–262.

[8] M. Sabbah, H. Keener, G. Meyer, Simulation of solar drying of shelled corn using the logarithmic model, Transactions of the ASAE 22 (3) (1979) 637–643.

[9] J. Sitompul, I. Istadi, I. Widiasa, Modeling and simulation of deep-bed grain dryers, Drying Technology 19 (2) (2001) 269–280.

[10] I. Istadi, J. Sitompul, A comprehensive mathematical and numerical modeling of deep-bed grain drying, Drying Technology 20 (6) (2002) 1123–1142.

[11] J. Sitompul, I. Istadi, S. Sumardiono, Modelling and simulation of momentum, heat, and mass transfer in a deep-bed grain dryer, Drying Technology 21 (2) (2003) 217–229.

[12] E. Herman-Lara, M. A. Salgado-Cervantes, M. A. Garcia-Alvarado, Mathematical simulation of convection food batch drying with assumptions of plug flow and complete mixing of air, Journal of Food Engineering 68 (3) (2005) 321–327.

[13] J. Cranck, The Mathematics of Diffusion, Oxford, 1956.

[14] G. Karniadakis, R. Kirby, Parallel Scientific Computing in C++ and MPI, Cambridge University Press, 2003.

[15] R Development Core Team, R: A Language and Environment for Statistical Computing, R Foundation for Statistical Computing, Vienna, Austria (2011).

[16] S. Janas, S. Boutry, P. Malumba, L. Vander Elst, F. Béra, Modelling dehydration and quality degradation of maize during fluidized-bed drying, Journal of Food Engineering 100 (3) (2010) 527–534.

[17] D. Zare, S. Minaei, M. Mohamad Zadeh, M. Khoshtaghaza, Computer simulation of rough rice drying in a batch dryer, Energy Conversion and Management 47 (18-19) (2006) 3241–3254.

[18] M. de Lemos, Turbulence In Porous Media, Elsevier, 2006.

[19] H. S. Perry, Chemical engineer's handbook, Mc Graw Hill.

[20] R. Earle, Unit Operations in Food Processing, Pergamon Press, 1983.

[21] D. Kunii, O. Levenspiel, Fluidisation engineering, Boston.

Websites

FAOSTAT : http://faostat.fao.org
GMM and GETFEM : http://download.gna.org/getfem/html/homepage/
GMSH : http://www.geuz.org/gmsh/